R. & M. No. 3291

MINISTRY OF AVIATION

AERONAUTICAL RESEARCH COUNCIL
REPORTS AND MEMORANDA

The Mixing of Free Axially-Symmetrical Jets of Mach Number 1·40

By

N. H. JOHANNESEN,
Department of the Mechanics of Fluids,
University of Manchester

LONDON: HER MAJESTY'S STATIONERY OFFICE
1962
PRICE 12*s*. 6*d*. NET

The Mixing of Free Axially-Symmetrical Jets of Mach Number 1·40

By

N. H. JOHANNESEN,

Department of the Mechanics of Fluids, University of Manchester

COMMUNICATED BY THE DIRECTOR-GENERAL OF SCIENTIFIC RESEARCH (AIR),
MINISTRY OF SUPPLY

Reports and Memoranda No. 3291*

January, 1957

Summary.—Axially-symmetrical, supersonic, fully-expanded jets of diameter about 0·75 in. and of Mach number 1·40 issuing into an atmosphere at rest were investigated by schlieren and shadow photography and by pressure traversing. The development of the jets was found to depend critically on the strength of the shock waves in the core of the jet at the nozzle exit. With strong shock waves present the jet spread very rapidly and was very unsteady. The jet did in some cases break up into large eddies of the same size as the diameter of the jet. When no disturbances were present in the core of the jet the spreading was far more gradual and the jet showed only slight unsteadiness. The turbulent mixing region of the first part of the jet with strong shock waves was investigated in detail by pitot tubes. The first inch was found to correspond to a two-dimensional half-jet. The velocity profiles were similar and well represented by the error integral. The rate of spreading was only half the value for low-speed flow. By integrations across the mixing region the entrainment and the loss of kinetic energy were determined. These quantities were found to agree well with the values estimated by assuming an error-integral velocity profile.

1. *Introduction.*—The flow in supersonic air jets has been the subject of a very large number of papers. In spite of this extensive literature our knowledge of the details of the flow is still very limited, mainly because most theoretical and experimental investigations until very recently were concerned almost exclusively with the pattern of shock and expansion waves which occurs in the jets and not with the development of the mixing region between the jet and the surrounding air.

This paper is a report on the first part of a research programme which was originally planned to study one of the simplest cases of supersonic jet mixing, namely that in which a uniform and parallel axially-symmetrical jet with no internal disturbances issues into an atmosphere at rest. As it happened, the problem of producing such a jet was found to be more difficult than anticipated, and the first nozzle produced a jet with strong internal shock waves. The attempts to improve the flow were eventually successful, and a nozzle was obtained which produced a jet with only very weak disturbances.

In the process of improving the flow it was found that the strength of the internal shock waves had a very marked effect on the development of the mixing region and thereby on the spreading of the jet. The jets with internal disturbances spread far more rapidly than did the uniform jet. The noise from the jet with internal shock waves was far greater than the noise from the jet with only weak internal disturbances.

* Previously issued as A.R.C. 18,967.

This problem of the effect of the internal disturbances on the mixing process was considered sufficiently important to warrant a more detailed investigation. This first report describes photographic investigations of both non-uniform and uniform jets together with a detailed investigation by pressure traverses of the jet with strong internal shock waves. The detailed investigation of the uniform jet is in progress and will be described later.

When a supersonic jet from an axially-symmetrical nozzle in which there is only a thin boundary layer issues into an atmosphere at rest, the flow may be divided roughly into three regions. Near the nozzle exit the mixing region is thin compared with its distance from the axis, and the flow is essentially that in a two-dimensional half-jet. Farther downstream the mixing region is no longer thin compared with its distance from the axis, but there is still a core in the jet unaffected by the mixing. This core eventually disappears and in the third region of the jet the mixing region extends across the whole of the jet.

Because of the extreme unsteadiness of the flow in this third region of the jet with strong internal disturbances, the pressure traverses could only be carried out successfully in the first two regions.

All jets discussed here had the same nominal Mach number of $1{\cdot}400$, and the exit diameters of the nozzles were all about $0{\cdot}75$ inches.

2. *Experimental Arrangement.*—(*a*) The air-supply system is shown schematically in Fig. 1. Air enters the two-stage compressor A from the atmosphere. After the compressor it passes through the oil separator B, the aftercooler C, the water separator D, and the dryer E to the reservoir G. F is a pressure control valve which keeps the pressure after the compressor at a constant value of 100 p.s.i. independent of the pressure in the reservoir. About 85 per cent of the water content is extracted before the air reaches the dryer, after which the dew point at atmospheric pressure is between $-30°$C and $-50°$C, corresponding to specific humidities between $0{\cdot}0002$ and $0{\cdot}00002$. The reservoir has a volume of 4,500 cu. ft. and supplies air to an 8 in. diameter pipe H whose end is closed by a flange J in which the nozzle K was mounted. The pipe and the flange were carefully adjusted so that the axis of the issuing jet was horizontal.

The nozzle diameter was chosen so that the capacity of the compressor slightly exceeded the mass flow through the nozzle for normal working pressures. The excess air escaped through an adjustable needle valve L. In this way it was possible to run the jet continuously and to keep the pressure just upstream of the nozzle, as measured on the manometer M, constant during a run. The practice adopted was to keep the pressure within ± 5 mm. Hg. of the desired value. In all the experiments described here, the ratio of stagnation pressure p_s to barometric pressure B was kept at the value corresponding to isentropic expansion to a Mach number of $1{\cdot}400$, *i.e.*, $p_s/B = 3{\cdot}183 \pm 0{\cdot}006$, corresponding to a maximum error of $\pm 0{\cdot}2$ per cent.

The reservoir is placed in the open air, and the experiments were carried out in a large room (a small hangar) with sliding doors which were kept open during the tests. The heat capacity of the piping and the reservoir (three Lancashire boilers) was large compared with that of the rate of flow of air, and it could therefore be assumed that the air leaving the reservoir was in temperature equilibrium with the surroundings so that the stagnation temperature just upstream of the nozzle was equal to the ambient temperature of the air into which the jet was issuing.

Some of the experiments described here were carried out before the dryer was installed, and the compressor pumped air directly into the reservoir. The air upstream of the nozzle was therefore saturated with water at room temperature. At the pressure of roughly 3 atm. abs. and a temperature of 10°C (typical for the experiments) this corresponds to a specific humidity of about $0{\cdot}0025$. It was expected that this humidity content would have only a small effect on the flow in the jet. After the dryer had been installed a number of experiments were repeated with dry air. No detectable differences were found between the results with wet air and those with dry air.

(*b*) *Schlieren Equipment.*— The schlieren photographs were taken with a conventional two-mirror schlieren system with a 5 in. diameter parallel beam passing through the jet. Three light sources were used : a continuous mercury-vapour source which was used with a mechanical shutter to give exposure times of the order 1/50 to 1/100 sec., a mercury-vapour flash tube with effective duration about 10 microseconds, and a spark gap with duration between $\frac{1}{2}$ and 1 microseconds. These light sources are in what follows referred to as continuous, flash, and spark source, respectively.

By removing the schlieren knife edge the optical set-up could also be used for direct shadow photography.

(*c*) *Traversing Arrangement.*—The jet was traversed at various stations with either a single pitot tube or a single static tube. Both tubes had outside diameters 0·040 in. and the pitot tube had an inside diameter of 0·025 in. The tubes were placed in a traversing gear which made it possible to move them across the jet in the horizontal plane of symmetry. The driving screw had 26 threads per inch, and the smallest steps used were 1/10 of a turn corresponding to 1/260 of an inch. In spite of the extra work involved, a single tube was used in preference to a rake of several tubes. The reason for this is discussed below. The pitot pressures were measured with a U-tube mercury manometer with one end open to the atmosphere, and the static pressures were measured with a similar water manometer.

In the earlier experiments with wet air considerable trouble was caused by the pitot tube getting blocked with ice. This made the experimental work almost impossible on very cold days. No such difficulties were present when dry air was used.

3. *Photographs.*—(*a*) *Foelsch Nozzles.*—In the experiments as originally planned it was intended to study the mixing of a uniform and parallel jet of a Mach number of 1·400 with the surrounding still air. A nozzle contour which it was hoped would satisfy this requirement was therefore calculated using the method due to Foelsch[3]. A boundary-layer displacement correction (to the radius) which increased linearly from zero at the throat to a, somewhat arbitrarily chosen, value of 0·009 in. at the exit was added to this contour. The Foelsch method does not give any information about the subsonic part of the nozzle, but the subsonic contour was chosen as a circular arc. All the nozzles 1 to 5 listed in Table 1 had the same supersonic contour.

TABLE 1

Nozzles

Nozzle	d_{throat}	d_{outlet}	Inlet radius
No.	inches	inches	inches
1	0·708	0·765	3/16
2	0·708	0·765	3/16
3	0·673	0·727	3/16
4	0·720	0·774	3/16
5	0·742	0·796	3·0
6	0·700	0·739	—

Photographs of the jet from Nozzle 1 (Jet 1) showed that the flow at the exit of the nozzle was far from uniform (*see* Figs. 2 to 5). In addition to a weak disturbance from the lip of the nozzle, a strong shock wave was seen to originate inside the nozzle. A similar shock wave had been observed earlier in the jet from a simple convergent-divergent nozzle with a conical outlet (*see* Ref. 7). It was not surprising that such a simple shape should give a flow with strong disturbances. The supersonic part of Nozzle 1 had, however, been designed to give a uniform flow without shock waves, and the reason for the occurrence of the strong shock wave was therefore

likely to be found in the shape of the subsonic inlet. It is obvious that the flow pattern in the supersonic part of the nozzle must depend on the subsonic approach : in particular, the Foelsch nozzle design method assumes a straight sonic line (a plane sonic surface) whereas in fact the ' camber ' of the sonic line is inversely proportional to the square root of the radius of curvature of the nozzle contour at the throat (Ref. 13). A small inlet radius will therefore lead to a strongly-curved sonic line. To make the sonic line flatter the inlet should either have a very large radius or the inlet should be faired very gradually into a nearly parallel throat.

A few experiments were carried out using Nozzles 2 to 5. Before discussing these experiments it is necessary to say a few words about the manufacture of such small nozzles.

The nozzles were of aluminium alloy and turned on a bench centre-lathe fitted with a home-made profiling attachment. The copying template was made to agree within 0·00025 in. with the theoretical ordinates, and the making of the template took about two weeks. With the template available a nozzle could be made in about one day, and the contour was estimated to be accurate to within 0·0005 in. Some difficulties were, however, experienced in getting the nozzle diameter right. This is the reason for the diameters of Nozzles 3 to 5 being as much as 5 per cent different from the correct values of Nozzles 1 and 2. Nozzles 3 to 5 were in fact just attempted nozzles which, as they were available anyway, were used for a few experiments, although they would not have been suitable for use in a main experiment.

Nozzle 2, which was identical with Nozzle 1, was used to verify that the shock wave did in fact originate just downstream of the throat, and was not caused by any irregularities in the supersonic part of the nozzle. The nozzle was shortened in steps from the supersonic end and photographs were taken at each stage.

In Nozzle 3 the fairing of the subsonic inlet into the throat region was made slightly more gradual than in Nozzle 1 but the flow in the jet was not visibly different.

In Nozzle 4 the inlet was faired into a short cylindrical throat region about 1/32 in. long, but this modification did not produce any detectable differences in the flow pattern.

However, in the jet from Nozzle 5, which had a large inlet radius of 3·0 in., the shock wave was definitely weaker than in the jets from the other nozzles. The flow patterns downstream in the jets were also substantially different in the jets from Nozzles 1 and 5. This is discussed in more detail below.

These experiments on the effects of the contours of the inlet and the throat region were not carried any further, because at that time a report on a similar and more detailed investigation carried out at the National Gas Turbine Establishment became available (Ref. 6). This report describes the calibration of a Foelsch design axially-symmetrical nozzle for a Mach number of 1·400 fitted with one of two different subsonic approach sections. The conclusions of the report emphasise the importance of choosing a subsonic approach which is designed so that the shape of the sonic surface at the throat agrees with the one specified in the particular supersonic-nozzle design method used.

(*b*) *Clippinger Nozzle.*—Although the jet from Nozzle 5 was far more uniform than the jet from Nozzle 1, it was felt that the original object of producing a uniform and parallel jet had not been achieved. A trial and error method of improving the shape of the nozzle was obviously going to be lengthy and was also unsatisfactory from a theoretical point of view.

It was therefore decided to try an entirely different design method, the one due to Clippinger[2]. We were fortunate in receiving from Mr. R. F. Sargent of the Bristol Aeroplane Company a complete set of isentropic ordinates for an axially-symmetric nozzle of Mach number 1·400 calculated by the Clippinger method. Assuming a laminar boundary layer, an estimate was made of the displacement thickness at the exit of a nozzle with these ordinates and a throat diameter of 0·700 in. The estimated value was 0·001 in., and as this is only slightly larger than the estimated maximum error in manufacture, no displacement-thickness correction was made for this nozzle (No. 6).

The jet from Nozzle 6 is shown in Figs. 6 to 9 and a comparison with Figs. 2 to 5 leaves no doubt about the improvement in the flow.

(*c*) *Discussion of Photographs.*—In all the schlieren photographs reproduced here the knife edge was vertical, *i.e.*, perpendicular to the axis of the jet and cutting off in such a way that regions with density increasing in the downstream direction appear dark on the photographs. Photographs were also taken with the schlieren knife edge parallel to the axis but in these the details of the flow patterns were partly obscured by the strong radial-density gradients in the mixing region, and they are therefore not reproduced here.

A general point to be noted about this series of photographs is the extreme dependence of the appearance of the pictures on the duration of the light source. The speed with which eddies in the flow are carried downstream can be taken to be roughly of the order of that of sound. For the three light sources used, namely continuous, flash and spark, this corresponds to displacement values of the order 100, 0·1 and 0·01 in., respectively. This explains the fact that the spark source appears to ' freeze ' the flow pattern whereas the flash photographs have a slightly ' woolly ' appearance. The long duration photographs show the mean flow only.

In Jet 1 a strong conical shock wave is seen to originate inside the nozzle. It forms a Mach shock at the axis about 0·3 in. downstream of the exit. The continuation of this shock wave meets the mixing region at $x = 0{\cdot}6$ in. and is reflected as an expansion fan. This expansion fan is reflected as a compression fan and the process is repeated farther downstream but becomes more and more affected by the spreading of the mixing region into the core of the jet and by the appearance of shock waves formed as envelopes of compression waves.

In interpreting the photographs it should be remembered that they do not represent a section through the jet but rather the integrated effects of the density gradients along the whole lengths of the light rays passing through the jet.

Close to the strong shock wave originating inside the nozzle a weak shock wave springs from the lip of the nozzle. This shock wave may be present because the boundary-layer allowance at the nozzle exit was too large, as will appear from the discussion of the pressure traverses, so that the air expanded inside the nozzle to a pressure slightly lower than that of the atmosphere.

In addition to these well defined shock waves, the whole flow is covered by a criss-cross pattern of very weak compression and expansion waves caused by minute irregularities in the surface of the nozzle.

Looking now at Jet 6, a similar criss-cross pattern will be seen, but the shock wave originating inside the nozzle and the one springing from the lip appear to be absent.

In the short-duration photographs it is clearly seen how very small irregularities in the mixing region break up into discrete eddies which grow in size as they are carried downstream. In Jet 1 these irregularities in the mixing region start almost at the exit of the nozzle, but in Jet 6 there is a short region with laminar flow just downstream of the nozzle. This is particularly clearly seen on Fig. 8. The most remarkable difference between the two jets is found in the rate of growth of the eddies and consequently in the spreading of the jets. It is obvious from the photographs that the spreading is far more rapid in Jet 1. This was confirmed by the pressure measurements which will be discussed in the following paragraph.

Photographs of Jet 1 also showed differences on an even larger scale. In some pictures the jet was seen to break up into what appeared on the photographs as definite eddies of a size of the same order as the diameter of the jet, but should probably more correctly be interpreted as a spiral vortex pattern. This breaking up into very large eddies was accompanied by a very rapid spreading of the jet farther downstream. In other photographs the spreading was more moderate and no very large eddies were present. This phenomenon is illustrated in Figs. 3 and 4 and is further discussed in the following paragraph.

4. *Pressure Traverses.*—(*a*) *Survey of Traverses.*—The jet from Nozzle 1 was traversed with the pitot tube in the horizontal plane of symmetry at the following values of x: 0, 0·1, 0·2, 0·3, 0·4, 0·5, 0·6, 0·8, 1·0, 1·5, 2·0, 2·5, 3·0, 4·0, 5·0, 6·0, 8·0 and 10·0 inches. Because of the small scale of the jet and because of the presence of shock waves it was not possible to make reliable static-pressure traverses near the nozzle exit. The static tube was therefore only traversed at the stations from $x = 3{\cdot}0$ in. to $x = 10{\cdot}0$ in.

The radial distance between consecutive pressure readings increased from 1/260 in. (1/10 turn) at $x = 0$ in. to 5/26 in. (5 turns) at $x = 10{\cdot}0$ in.

The pitot pressure H and the static pressure p were made non-dimensional by dividing by the barometric pressure B. H/B and p/B were plotted against distance across the jet with an arbitrary zero which, of course, at each station was the same for both pitot and static pressures.

Typical pressure traverses for $x = 0{\cdot}4$ in. and $x = 10{\cdot}0$ in. are shown in Figs. 10 and 11. In these graphs the distance from the axis is given in terms of the nozzle exit radius r_N.

The investigation of the jet from Nozzle 6 has not yet been completed, but as a comparison the traverses at $x = 0{\cdot}4$ in. and $x = 10{\cdot}0$ in. are included in Figs. 10 and 11.

From graphs similar to those in Figs. 10 and 11, but plotted with arbitrary zero for the distance across the jet, the axis of symmetry of the profiles could be determined. This method was very accurate for $x \leqslant 2{\cdot}5$ in. but became less accurate for larger values of x. It is felt that this method of finding the centre of the jet at each traversing station gives far higher accuracy than could have been obtained by relating the position of the pitot tube to the axis of the nozzle. The use of a rake of pitot tubes would also have led to difficulties in determining the relative positions of the individual pitot tubes with sufficient accuracy. In the method used, the position of the centre of each traverse could for $x \leqslant 2{\cdot}5$ in. be determined with an accuracy of from 0·0001 to 0·0005 in., but this accuracy does not necessarily give a true impression of the actual accuracy of the experimental results because of the possible pitot-tube displacement effect. It was felt that insufficient information is available about this effect in supersonic shear flow, and it was therefore assumed that the reading always corresponded to the geometrical centre of the pitot tube.

An exception was the traverse at $x = 0{\cdot}0$ in. where the pitot tube was moved in the plane of the nozzle exit. When the pitot tube was moved towards the centre of the jet the manometer recorded a pressure as soon as part of the pitot tube opening was inside the circumference of the nozzle exit although the centre of the pitot tube was still outside the circumference. It was assumed that the pressure read was that at a point half way across the exposed part of the pitot-tube opening. This displacement correction was therefore 0·0125 in. at the outer edge of the jet and decreased to zero in a distance of 0·025 in.

The mercury manometer was in all cases read to the nearest millimetre. For the traverses up to $x = 2{\cdot}5$ in. the readings were very steady and the readings were repeatable. However, from $x = 3{\cdot}0$ in. and outwards the mercury columns fluctuated. At $x = 3{\cdot}0$ in. the fluctuations were confined to the outer edge of the jet, but as x was increased the fluctuations spread to the whole of the jet and increased in magnitude. Readings were taken by estimating the mean values on the manometer, but this procedure became increasingly difficult as x was increased.

As an example Fig. 12 shows the variation of the manometer reading of H/B with time for four periods each of one minute's duration. The pitot tube was in each case placed at $x = 5{\cdot}0$ in. and approximately on the axis of the jet. When the pitot tube was moved away from the axis the relative fluctuations in the difference $H - B$ became larger and near the edge they were several times the mean value.

When the estimated average values obtained at stations from $x = 3{\cdot}0$ in. and downstream were used to obtain velocity profiles and to calculate the flow quantities in the jet, the final results were very erratic. A number of traverses were repeated but the agreement with the

previous results was poor. It was concluded that the method of measurement was inadequate and the results for $x \geqslant 3{\cdot}0$ in. have not been included in the present report. It was felt, however, that the irrepeatability of the results was not satisfactorily explained by the measuring difficulties. There was some indication that the flow pattern in the downstream part of the jet did in fact change from day to day.

On the records in Fig. 12 it will be noticed that in addition to the small fluctuations there are 'bursts' of large variations in the pressure. On the particular day when these records were obtained these bursts occurred at intervals of the order of one minute. This indicates that the structure of the jet was changing with a very low frequency or perhaps rather that periods of relative calm were followed by short violent oscillations of the flow, a phenomenon not unlike the intermittency at the edge of a turbulent jet (*see* Ref. 15). It should be remembered, however, that these pressure records were taken at the axis of the jet, so that the intermittency in the flow must have been present in the whole of the jet. When the jet was observed on the schlieren screen, low frequency changes in the flow pattern could also be observed. They appeared not as oscillations of the jet as a whole but rather as a series of abrupt changes in the angle of spread of the jet, as if the jet was contracting and expanding laterally with its axis remaining fixed. Such oscillations would of course result in oscillations of the pressure on the axis even if the axis remained fixed. This phenomenon has already been mentioned in the preceding paragraph and examples are shown in Figs. 3 and 4. In Fig. 3 two photographs are given of the jet near the exit, and Fig. 4 shows two photographs of the jet farther away from the nozzle. The differences in the angle of spread of the jet are clearly visible, and it is also clear that the breaking up into large eddies is followed by very rapid spreading.

These phenomena were not investigated in detail, but it seems possible that the rate of spreading of the jet may have changed not only during an experiment but also from day to day, for reasons not fully understood. This would account for the inconsistency of the experimental results for x greater than $2{\cdot}5$ in. It might be mentioned that sudden changes in the manometer reading were accompanied by changes in the noise of the jet. This noise was most of the time of no definite pitch, but short periods did occur during which a definite tone was superimposed on the random noise.

A fuller investigation of the fluctuations in Jet 1 would obviously be very interesting but the present experimental equipment was not suitable for such work, and we must therefore confine ourselves to these few qualitative remarks.

Pressure traverses made so far of Jet 6 indicate that even at $x = 10$ in. the flow is steady with only very small fluctuations in the pitot-pressure readings. The audible noise from Jet 6 is also very much smaller than that from Jet 1.

(*b*) *Velocity Profiles.*—If both pitot and static pressures are known, the Mach number can be found from well known text-book relations which have been tabulated (*see*, for example, Ref. 12). If furthermore the stagnation temperature T_s is known, the local temperature T is found from the Mach number as

$$T = T_s \left(1 + \frac{\gamma - 1}{2} M^2\right)^{-1} \quad \ldots \quad \ldots \quad \ldots \quad \ldots \quad \ldots \quad \ldots \quad (1)$$

As mentioned above, in the present experiments the stagnation temperature upstream of the nozzle was always equal to the temperature of the atmosphere into which the jet was issuing. It was therefore assumed that the stagnation temperature was equal to room temperature everywhere.

The velocity ratio is then

$$\frac{U}{U_1} = \left(\frac{T_s - T}{T_s - T_1}\right)^{1/2} = \frac{M}{M_1}\left(\frac{1 + \frac{\gamma - 1}{2} M_1^2}{1 + \frac{\gamma - 1}{2} M^2}\right)^{1/2} \quad \ldots \quad \ldots \quad \ldots \quad (2)$$

where suffix 1 refers to the values at the inner edge of the mixing region. We notice that the velocity ratio is independent of the actual value of T_s, as long as T_s is assumed constant across the mixing region.

As the present discussion deals only with the conditions in the jet for values of x less than or equal to 2·5 in., no static pressures were available. This meant that it was not possible to determine the Mach number or the velocity profiles across the core of the jet where shock waves were present and obviously caused variations in both static pressure and flow direction. In the mixing region near the edge of the jet the static-pressure variations are likely to have been very small, and it was therefore assumed that the static pressure was constant and equal to the barometric pressure B. This assumption may not be correct at values of x where strong shock waves interact with the mixing region.

Using the values of H/B found from the pressure traverses, the non-dimensional velocity profiles were plotted against distance across the jet with the same arbitrary zeros as were used for plotting H/B, leaving out the core of the jet. From these graphs the axis of symmetry of each profile was again determined and as a check the values were compared with those found from the H/B curves.

For use later the absolute value of U_1 for each value of x was also determined.

The non-dimensional velocity profiles are shown in Fig. 13. Fig. 14 shows the profiles in the first inch of the jet on a larger scale. The first three profiles at $x = 0·0$, $0·1$ and $0·2$ inches are shown on a still larger scale in Fig. 15 to demonstrate the rapid change from a boundary-layer profile to a free mixing-region profile.

(*c*) *Similarity of Profiles.*—In the theoretical solutions of turbulent-mixing problems the velocity ratio is expressed as a function of a non-dimensional distance across the jet

$$\frac{U}{U_1} = F\left(\sigma \frac{y'}{x'}\right). \quad \ldots \quad \ldots \quad \ldots \quad \ldots \quad \ldots \quad \ldots \quad \ldots \quad \ldots \quad (3)$$

As zero for y' we shall use the value of r at which $U/U_1 = 0·5$. The co-ordinate x' is the distance from a virtual origin, and σ is a scale factor which has to be determined experimentally. In the theories σ is independent of x' and y' but depends on some other parameter such as the ' mixing length ' or the eddy viscosity.

To investigate whether the experimentally determined velocity profiles are similar, the virtual origin, *i.e.*, the zero for x', must first be determined. This was done by plotting mixing-region width Δy against x, the distance from the exit of the nozzle. It appears that a number of different definitions of Δy have been used. Three of these were used in the present investigation, namely

$(\Delta y)_a$ the difference between the values of r at which U/U_1 equals $0·1$ and $0·9$, respectively.

$(\Delta y)_b$ the difference between the values of r at which $(U/U_1)^2$ equals $0·1$ and $0·9$, respectively. These values of $(U/U_1)^2$ correspond to values of U/U_1 of $0·316$ and $0·949$, respectively.

$(\Delta y)_c$ the difference between the values of r at which U/U_1 equals $0·1$ and $0·95$, respectively.

When these three different measures of the mixing-region width were plotted against x it was found that the points fell in two distinct groups, within each of which the variation with x was nearly linear.

Fig. 16 shows the results for Group I for which x varies from $0·1$ to $1·0$ in., and Fig. 17 those for Group II for which x varies from $1·0$ to $2·5$ in. The best straight line was fitted to each

series of points. If the profiles were exactly similar the three lines within each group would intersect the x-axis at a single point. This is seen to be very nearly the case for Group I, but for Group II the virtual origin is less well defined.

The average values of the zeros of x' were used. They were for Group I, $x = -0{\cdot}23$ in. and for Group II, $x = +0{\cdot}31$ in.

The velocity profiles were compared with the simple expression

$$\frac{U}{U_1} = F_1\left(\sigma\frac{y'}{x'}\right) = \frac{1}{2}\left[1 + \text{erf}\left(\sigma\frac{y'}{x'}\right)\right] \quad .. \quad .. \quad .. \quad .. \quad .. \quad (4)$$

where $\text{erf}\,(t) = \int_0^t \frac{2}{\sqrt{\pi}} \exp\,(-t^2)\,dt$, and with the tabulated function F_2 given by Görtler[5] who calculated the velocity profile for an incompressible turbulent half-jet assuming constant eddy viscosity. F_2 was found as a series solution the first term of which is equal to F_1. (Our F_1 and F_2 are not the same as F_1 and F_2 in Görtler's notation.)

The best values of σ were found as the ratios of the theoretical values of $\sigma\Delta y/x'$ to the means of the experimental values of $\Delta y/x'$. Average values of σ were used. They were for Group I, $\sigma = 21{\cdot}9$ and for Group II, $\sigma = 11{\cdot}9$.

Figs. 18 and 19 show U/U_1 plotted against $\sigma y'/x'$ for each of the two groups, and it will be seen that the velocity profiles exhibit a high degree of similarity. Apart from the values at $x = 1{\cdot}0$ in. which fit well into Group I only, the scatter can easily be accounted for by experimental inaccuracies. The maximum deviation from a mean curve (not shown) is $\pm 0{\cdot}01$ in U/U_1, except near the outer edge of the mixing region. Fig. 18 is particularly remarkable in view of the fact that $r_{0{\cdot}1} - r_{0{\cdot}9}$ is only $0{\cdot}028$ in. at $x = 0{\cdot}1$ in., that is about the same as the diameter of the pitot-tube opening and considerably smaller than the outside diameter of the pitot tube. That the profiles are true profiles is supported by the experiments by Johannesen and Mair[8] who found that the measured distribution of pitot pressure across a supersonic wake was independent of pitot-tube size as long as the outside diameter of the pitot tube was less than about twice the width of the wake.

In Group I the flow is essentially that in a half-jet, and Fig. 18 may therefore be compared with Fig. 13 in the paper by Liepmann and Laufer[9] who investigated the incompressible half-jet. It will be seen that the relative scatter is of the same order in the two cases although the width of the mixing region in our case is only about one fiftieth of that in the low-speed results of Liepmann and Laufer.

The experimental values in Fig. 18 approximate rather better to Görtler's curve, F_2, than to F_1, but in Fig. 19 the points for $x = 1{\cdot}5$, $2{\cdot}0$ and $2{\cdot}5$ inches are very closely approximated by F_1 except at the outer edge of the mixing region. We shall see later, however, that the simple function F_1 is a fully adequate representation of the velocity profiles in Group I when it is used to calculate the flow quantities in the mixing region.

The value of $\sigma = \widehat{21{\cdot}9}$ for the points in Group I should be compared with the value of $\sigma = 11{\cdot}0$ found by Liepmann and Laufer for incompressible flow. For the first part of the jet where the flow is very nearly that in a half-jet we have thus found that at a Mach number of $1{\cdot}4$ the rate of spreading is almost exactly half the value in incompressible flow.

The fact that the points in Group I fit F_2 rather better than F_1 is not considered to be of any great significance. It is important, however, that an increase in speed from a low subsonic Mach number to a Mach number of $1{\cdot}4$ changes the value of σ only, but leaves the velocity profile unchanged within the experimental accuracy.

Two experimental investigations of mixing in a supersonic half-jet have been published. In both cases density profiles were measured by an interferometer and the experimental scatter was considerably larger than in the present experiments.

Gooderum, Wood and Brevoort[4] found a value of $\sigma = 15$ for a Mach number of $1 \cdot 60$ when comparing their experimental velocity profiles with the theoretical curve for incompressible flow due to Tollmien[14].

Bershader and Pai[1] found $\sigma = 17$ when their experimental density profiles were compared with a theoretical curve calculated using the theory of supersonic mixing developed by Pai[10].

No experimental values are available for comparison with the value of $\sigma = 11 \cdot 9$ found for Group II. In this region the jet is neither of the half-jet type nor of the fully-developed axially-symmetric type. The fact that σ changes very rapidly in the neighbourhood of $x = 1 \cdot 0$ in. is no doubt caused by the interactions between the mixing region and the disturbances in the core of the jet.

(*d*) *The Ideal Jet.*—Before we proceed with the treatment of the experimental results it is necessary to discuss the effect of day-to-day variations in the experimental conditions.

The non-dimensional flow quantities in the jet, such as velocity ratios, mixing-region width in terms of nozzle exit radius, etc., will depend on two non-dimensional parameters, a Mach number taken, for example, on the axis of the jet in the exit plane of the nozzle, and a Reynolds number defined, for example, by the velocity and kinematic viscosity at the same point together with the radius of the nozzle outlet.

In the experiments the reference Mach number was always the same because the pressure ratio across the nozzle was always that corresponding to isentropic expansion to a Mach number of $1 \cdot 400$. The reference Reynolds number did, however, vary from day to day because of the variations in atmospheric pressure and temperature. The variation in Reynolds number was small, the maximum deviation from the mean value being ± 3 per cent. It is well known that the non-dimensional quantities, such as for example pressure ratios, vary very slowly with Reynolds number, and it therefore seems fully justified to assume that the non-dimensional pressure profiles were independent of the day-to-day variations in atmospheric conditions.

This was in fact already assumed in the preceding paragraph where the velocity profiles obtained for different values of x and on different days were all assumed to belong to the same jet.

In what follows it will throughout be assumed that the non-dimensional quantities are typical for a jet from Nozzle 1 with correct pressure ratio and issuing into an atmosphere with pressure and temperature at values within those occurring during the experiments, *i.e.*, 750 to 770 mm. Hg and 10 to 20°C.

To make quantities such as velocity, mass flux, momentum flux, and kinetic-energy flux non-dimensional they are divided by the corresponding values in the exit plane of Nozzle 1 assuming isentropic flow and the atmospheric conditions prevailing at the time of the experiments. These ' ideal ' quantities are indicated by a suffix *1*.

When, however, actual numerical values are quoted they refer to a jet issuing into an atmosphere at normal pressure and temperature, *i.e.*, 760 mm. Hg and 0°C.

(*e*) *Velocity at Inner Edge of Mixing Region.*—Although the experimental scatter was found to be large for x greater than $2 \cdot 5$ in. it is of some interest to compare the axial variations of velocity for Jets 1 and 6. These are shown in Fig. 20, where the ratio U_1/U_i is plotted against distance from the exit measured in nozzle outlet radii. U_i is the ideal velocity at the exit and U_1 is the velocity at the inner edge of the mixing region, or, when the core has disappeared, the velocity on the axis. We notice the large difference between the two jets. A composite curve including several low-speed experiments on turbulent round jets was given by Townsend[15] and this curve is also shown in Fig. 20.

(*f*) *Integrations Across the Mixing Region.*—Let us first consider the two-dimensional case of a half-jet, Fig. 21. At a certain value of x, let y_0 and y_1 be the values of y for which the *experimentally* determined values of U/U_1 are 0 and 1, respectively. The position of the x-axis

is not important, but we shall assume that y_0 and y_1 are both positive. For a fixed value of x, the rate of mass flow Q, the momentum flux R, and the kinetic-energy flux K through the mixing region are, per unit width

$$Q = \int_{y_1}^{y_0} \rho\, U\, dy \qquad (5)$$

$$R = \int_{y_1}^{y_0} \rho\, U^2\, dy \qquad (6)$$

$$K = \tfrac{1}{2} \int_{y_1}^{y_0} \rho\, U^3\, dy\,. \qquad (7)$$

Because mass is continuously being added to the mixing region the displacement thickness does not seem to be a significant parameter. We may, however, define a momentum thickness δ_2 and an energy thickness δ_3 by the equations

$$\delta_2 = \int_{y_1}^{y_0} \left(1 - \frac{U}{U_1}\right) \frac{\rho U}{\rho_1 U_1}\, dy \qquad (8)$$

$$\delta_3 = \int_{y_1}^{y_0} \left(1 - \frac{U^2}{U_1^2}\right) \frac{\rho U}{\rho_1 U_1}\, dy\,. \qquad (9)$$

Q, R and K are insensitive to small variations in y_0. They do, however, depend critically on the choice of y_1, and we have

$$\left.\begin{aligned} \Delta Q &= -\rho_1 U_1 \Delta y_1 \\ \Delta R &= -\rho_1 U_1^2 \Delta y_1 \\ \Delta K &= -\tfrac{1}{2}\rho_1 U_1^3 \Delta y_1 \end{aligned}\right\} \qquad (10)$$

δ_2 and δ_3 are insensitive to small variations in either y_0 or y_1.

δ_2 and δ_3 are related to Q, R and K by the expressions

$$\delta_2 = \frac{1}{\rho_1 U_1^2}\,(QU_1 - R) \qquad (11)$$

$$\delta_3 = \frac{1}{\rho_1 U_1^3}\,(QU_1^2 - 2K)\,. \qquad (12)$$

As Q, R and K depend on the values of the integration limits and therefore on the experimental accuracy, they are not suitable characteristics of the mixing region. δ_2 and δ_3 do not, on the other hand, depend critically on y_0 and y_1, and they are therefore characteristics of the mixing region. To see their physical significance, we define the quantities E and D, where

$$E = \rho_1 U_1 \delta_2 \qquad (13)$$

$$D = \tfrac{1}{2}\rho_1 U_1^3\,(\delta_3 - \delta_2) \qquad (14)$$

we see that

$$E = Q - \frac{R}{U_1} \qquad (15)$$

and

$$D = \tfrac{1}{2}(Q - E)U_1^2 - K\,. \qquad (16)$$

R/U_1 is that part of the mass flow in the mixing region which originates from the core of the jet, and E is therefore the total mass entrained per unit time between the nozzle exit and the station considered. Similarly, $\frac{1}{2}(Q - E)U_1^2$ is the kinetic energy supplied to the mixing region from

the core. D is therefore the loss in kinetic energy in the mixing region at the station considered. This is not in practice equal to the total kinetic energy dissipated because some of the kinetic energy will be present in the form of turbulent energy.

In the axially-symmetric case we have (Fig. 22)

$$Q = 2\pi \int_{r_1}^{r_0} r\rho U \, dr \quad .. \quad .. \quad .. \quad .. \quad .. \quad .. \quad (17)$$

$$R = 2\pi \int_{r_1}^{r_0} r\rho U^2 \, dr \quad .. \quad .. \quad .. \quad .. \quad .. \quad .. \quad (18)$$

$$K = \pi \int_{r_1}^{r_0} r\rho U^3 \, dr \, . \quad .. \quad .. \quad .. \quad .. \quad .. \quad .. \quad (19)$$

In analogy with the two-dimensional case we may define a momentum area Δ_2 and an energy area Δ_3 by the equations

$$\Delta_2 = 2\pi \int_{r_1}^{r_0} r \left(1 - \frac{U}{U_1}\right) \frac{\rho U}{\rho_1 U_1} \, dr \quad .. \quad .. \quad .. \quad .. \quad (20)$$

$$\Delta_3 = 2\pi \int_{r_1}^{r_0} r \left(1 - \frac{U^2}{U_1^2}\right) \frac{\rho U}{\rho_1 U_1} \, dr \, . \quad .. \quad .. \quad .. \quad .. \quad (21)$$

Q, R and K are insensitive to small variation in r_0. They depend critically on r_1, and we have

$$\Delta Q = -2\pi r_1 \rho_1 U_1 \Delta r_1$$

$$\Delta R = -2\pi r_1 \rho_1 U_1^2 \Delta r_1$$

$$\Delta K = -\pi r_1 \rho_1 U_1^3 \Delta r_1 \quad .. \quad .. \quad .. \quad .. \quad .. \quad (22)$$

Δ_2 and Δ_3 are insensitive to small variation in either r_0 or r_1. Δ_2 and Δ_3 are related to Q, R and K by the expressions

$$\Delta_2 = \frac{1}{\rho_1 U_1^2} (QU_1 - R) \quad .. \quad .. \quad .. \quad .. \quad .. \quad (23)$$

$$\Delta_3 = \frac{1}{\rho_1 U_1^3} (QU_1^2 - 2K) \, . \quad .. \quad .. \quad .. \quad .. \quad .. \quad (24)$$

In analogy with the two-dimensional case we define

$$E = \rho_1 U_1 \Delta_2 \quad .. \quad .. \quad .. \quad .. \quad .. \quad .. \quad .. \quad (25)$$

$$D = \tfrac{1}{2} \rho_1 U_1^3 (\Delta_3 - \Delta_2) \, . \quad .. \quad .. \quad .. \quad .. \quad .. \quad (26)$$

As in the two-dimensional case it is possible to define momentum and energy thickness with reference to a characteristic length such as, for example, $r_{0 \cdot 5}$, the value of r at which $U/U_1 = 0 \cdot 5$. We then have

$$\delta_2 = \frac{\Delta_2}{2\pi r_{0 \cdot 5}}$$

and a similar expression for δ_3. In axially-symmetrical flow it is, however, more convenient to use the areas except in cases where δ_2 and δ_3 are very small compared with $r_{0 \cdot 5}$.

Using the two-dimensional equations, δ_2 and δ_3 were found for the velocity profiles given by F_1 and F_2 using numerical integration (Simpson's rule). The results were

For F_1 : $$\delta_2 = 0{\cdot}317x'/\sigma \quad .. \quad .. \quad .. \quad .. \quad .. \quad .. \quad (27)$$

$$\delta_3 = 0{\cdot}483x'/\sigma \quad .. \quad .. \quad .. \quad .. \quad .. \quad .. \quad (28)$$

$$\delta_3 - \delta_2 = 0{\cdot}166x'/\sigma \quad .. \quad .. \quad .. \quad .. \quad .. \quad .. \quad (29)$$

For F_2 : $$\delta_2 = 0{\cdot}321x'/\sigma \quad .. \quad .. \quad .. \quad .. \quad .. \quad .. \quad (30)$$

$$\delta_3 = 0{\cdot}471x'/\sigma \quad .. \quad .. \quad .. \quad .. \quad .. \quad .. \quad (31)$$

$$\delta_3 - \delta_2 = 0{\cdot}150x'/\sigma\,. \quad .. \quad .. \quad .. \quad .. \quad .. \quad .. \quad (32)$$

The last figure in these values is of doubtful significance because of the inaccuracy of the numerical integration method, and the difference between the results for F_1 and those for F_2 is therefore hardly significant. It should be noted that δ_2 and δ_3 are functions of M_1, and the values given here are therefore only correct for $M_1 = 1{\cdot}4$.

Using the three-dimensional equations, Q, R, K, E and D were determined by numerical integration of the experimental values for each value of x, but only the values of E and D are given here, because Q, R and K depend critically on the experimental values of r_1.

The integrations could be carried out directly. U/U_1 had already been determined, and from the equation of state we have, assuming that the pressure was constant across the mixing region,

$$\rho/\rho_1 = T_1/T = \frac{T_1}{T_s}\frac{T_s}{T}$$

where T_s/T is given by equation (1).

The non-dimensional values E/Q_i are shown in Figs. 23 and 24. The best straight lines are fitted to the points in each of the two groups. For the points in Group I it is a reasonable approximation to assume that the flow is two-dimensional, and we therefore have

$$E = 2\pi r_{0{\cdot}5}\delta_2\rho_1 U_1\,. \quad .. \quad .. \quad .. \quad .. \quad .. \quad .. \quad (33)$$

Using the mean values of $r_{0{\cdot}5}$, ρ_1, and U_1 and substituting the value of δ_2 from equation (27) or equation (30) we get the theoretical line shown dashed in Fig. 23. The difference between the results obtained from F_1 and F_2 is so small that it does not show up on the graph.

The non-dimensional values of D/K_i are shown in Figs. 25 and 26. The best straight lines are fitted to the points in each of the two groups. For the points in Group I we have

$$D = \pi r_{0{\cdot}5}(\delta_3 - \delta_2)\rho_1 U_1^3\,. \quad .. \quad .. \quad .. \quad .. \quad .. \quad (34)$$

The line corresponding to F_1 is shown dashed, and the one corresponding to F_2 is shown dotted.

It will be seen that both the entrainment and the loss of kinetic energy, for the part of the jet in which the flow is nearly two-dimensional, can be calculated with sufficient accuracy using the simple velocity profile given by F_1. The value of σ must, however, be determined experimentally.

From the calculated values of the entrainment, the rate of entrainment and hence the radial inflow velocity can be calculated. At a distance of one nozzle exit radius from the axis the velocity was found to be, for the first inch of the jet, 37 ft/sec.

The velocity profile at $x = 0{\cdot}0$ in. was used to determine the displacement thickness of the boundary layer at the exit of the nozzle. It was found to be $0{\cdot}006$ in.

(*g*) *Integrations across the Jet.*—Although the conditions across the core of the jet are not known accurately, they may be approximated by assuming that they are on the average equal to the conditions at the inner edge of the mixing region. With this assumption, the total values Q_t, R_t and K_t of the rate of mass flow, momentum flux, and kinetic-energy flux were calculated at each value of x. Fig. 27 shows the ratios Q_t/Q_i, R_t/R_i and K_t/K_i where, Q_i, R_i and K_i are the values for the ideal jet. The mass flow increases and the kinetic energy decreases with x increasing whereas R remains nearly constant. All curves show a kink at $x = 0{\cdot}6$ in. This is probably due to errors in the pitot pressure caused by the interaction of the shock wave with the mixing region.

5. *General Discussion and Conclusions.*—Two main problems have been investigated in detail, namely the effect of the strength of the internal disturbances on the development of the jet, and the detailed structure of the mixing region immediately downstream of the nozzle exit.

All the jets investigated were of a nominal Mach number of 1·400, and the nozzle area ratios were approximately at the correct value for isentropic expansion to this Mach number. The disturbances in the jet originated inside the nozzle and were not, as is more often the case, caused by the pressure at the exit of the nozzle being different from that in the atmosphere.

Strong internal shock waves, as in Jet 1, were found to cause a very rapid increase in the rate of spreading of the jet. In some cases the jet broke up into what appeared as large eddies of about the same size as the diameter of the jet. The mechanism of this eddy formation is not understood. It may, however, be a phenomenon similar to that observed by Powell[11] in two-dimensional jets for which the exit pressure was higher than the atmospheric pressure.

The present series of experiments shows that a certain strength of the shock waves in the jet is necessary for the formation of the large eddies. They were present in all the jets from the Foelsch design nozzles except from Nozzle 5 in which the shock waves were reduced in strength.

The first part of the mixing region of Jet 1 was investigated by pitot traversing. The results show a surprisingly small scatter in view of the small scale of the flow. This consistency of the results does not, however, necessarily mean that the results are highly accurate. There are a number of possible sources of errors which would cause systematic deviations from the true values without necessarily giving random scatter in the experimental results. Firstly, the static pressure was assumed constant across the mixing region. This is likely to be nearly correct, and the effect of the possible errors on the non-dimensional velocity profiles is likely to be small. Secondly, no pitot-tube displacement correction was applied to the results. If there were such a correction it would seem likely that its effect would have been dependent on the width of the mixing region and it should therefore have shown up on the graphs (Figs. 18 and 19) on which the velocity profiles are plotted with the same non-dimensional width. No systematic variation with mixing-region width is detectable, and it is therefore likely that the correction, if any, is smaller than the experimental scatter. Thirdly, no correction was made for the effect of turbulence on the reading of the pitot tube. This correction is likely to be small over the major part of the mixing region, but is no doubt significant near the outer edge. In this region the scatter of the experimental results is large, anyway, and the correction, if it had been known, would not have altered the over-all picture significantly. In low-speed flow Liepmann and Laufer[9] found that mean-velocity distributions measured with pitot tubes and with hot wires were in excellent agreement for values of U/U_1 greater than 0·2.

The velocity profiles between $x = 0{\cdot}1$ in. and $2{\cdot}5$ in. were found to fall into two distinct groups within each of which the spread was linear. In both groups the velocity profiles were well approximated by the simple expression of equation (4). The scale factor σ was 21·9 for Group I (0·1 in. $\leqslant x \leqslant$ 1·0 in.) and 11·9 for Group II (1·0 in. $\leqslant x \leqslant$ 2·5 in.).

The flow in the first inch of the mixing region was approximately that in a two-dimensional half-jet and the value of 21·9 for σ could therefore be compared with the low-speed value which lies between 11 and 12. This shows that the rate of spreading at a Mach number of 1·4 is only about half of what it is in low-speed flow.

For the first inch of the jet the experimentally determined values of the entrainment and the loss in kinetic energy were shown to be sufficiently accurately represented by assuming the simple velocity profile of equation (4).

The investigation of the uniform jet (Jet 6) had not yet been completed but a later report will deal with this jet in more detail.

Acknowledgements.—The photographic investigations described in this report were started by Dr. I. M. Hall who also designed the Foelsch nozzles. Mr. G. Artingstall assisted with the photographic work and the pressure measurements.

NOTATION

B	Barometric pressure
D	Loss of kinetic energy
E	Mass entrained
F_1	Function defined by equation (4)
F_2	Görtler's velocity profile
H	Pitot pressure
K	Kinetic-energy flux
M	Mach number
Q	Rate of mass flow
R	Momentum flux
T	Absolute temperature
U	Velocity
d	Diameter
p	Static pressure
r	Radius (distance from axis of jet)
x	Distance from nozzle exit
x'	Distance from virtual origin
y	Distance across jet
y'	Distance from point where $U/U_1 = 0{\cdot}5$
γ	Ratio of specific heats
δ_2	Momentum thickness
δ_3	Energy thickness
ρ	Density
σ	Scale factor {equation (3)}
Δ_2	Momentum area
Δ_3	Energy area

Suffixes

N	Nozzle exit
i	Ideal values
s	Stagnation values
t	Total values
0	Values at $U/U_1 = 0$
$0{\cdot}5$	Values at $U/U_1 = 0{\cdot}5$
1	Values at $U/U_1 = 1{\cdot}0$

REFERENCES

No.	*Author*	*Title, etc.*
1	D. Bershader and S. I. Pai	On turbulent jet mixing in two-dimensional supersonic flow. *J. App. Phys.* Vol. 21. p. 616. 1950.
2	R. F. Clippinger	Supersonic axially symmetric nozzles. Ballistic Research Laboratory, Report 794. 1951.
3	K. Foelsch	The analytical design of an axially symmetric Lavel nozzle for a parallel and uniform jet. *J. Ae. Sci.* Vol. 16. pp. 161 to 166 and 188. 1949.
4	P. B. Gooderum, G. P. Wood and M. J. Brevoort	Investigation with an interferometer of the turbulent mixing of a free supersonic jet. N.A.C.A. Report 963. 1950.
5	H. Görtler	Berechnung von Aufgaben der freien Turbulenz auf Grund eines neuen Näherungansatzes. *Z. angew. Math. Mech.* Vol. 22. pp. 244 to 254. 1942.
6	R. Hawkins	The influence of the subsonic approach contour on the Mach number and pressure distributions at the outlet of an axially symmetric supersonic nozzle. N.G.T.E. Note 26. 1954.
7	N. H. Johannesen	Study of high speed airflow by the schlieren method. *Oil.* (Journal of the Manchester Oil Refinery Group of Companies.) Vol. 4. No. 2. 1958.
8	N. H. Johannesen and W. A. Mair	Experiments with large pitot tubes in a narrow supersonic wake. *J. Ae. Sci.* Vol. 19. pp. 785 to 787. 1952.
9	H. W. Liepmann and J. Laufer ..	Investigations of free turbulent mixing. N.A.C.A. Tech. Note 1257. 1947.
10	S. I. Pai	Two-dimensional jet mixing of a compressible fluid. *J. Ae. Sci.* Vol. 16. pp. 463 to 469. 1949.
11	A. Powell	On the noise emanating from a two-dimensional jet above the critical pressure. *Aero. Quart.* Vol. 4. pp. 103 to 122. 1953.
12	L. Rosenhead (editor)	*Compressible airflow: Tables.* Oxford University Press. 1952.
13	R. Sauer	General characteristics of the flow through nozzles at near critical speeds. N.A.C.A. Tech. Memo. 1147. 1947.
14	W. Tollmien	Berechnung der turbulenten Ausbreitungsvorgänge. *Z. angew. Math. Mech.* Vol. 4. p. 468. 1926.
15	A. A. Townsend	*The structure of turbulent shear flow.* Cambridge University Press. 1956.

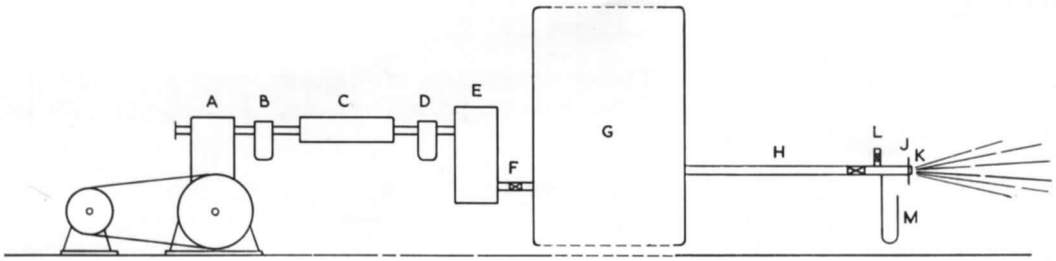

FIG. 1. Air-supply arrangement.

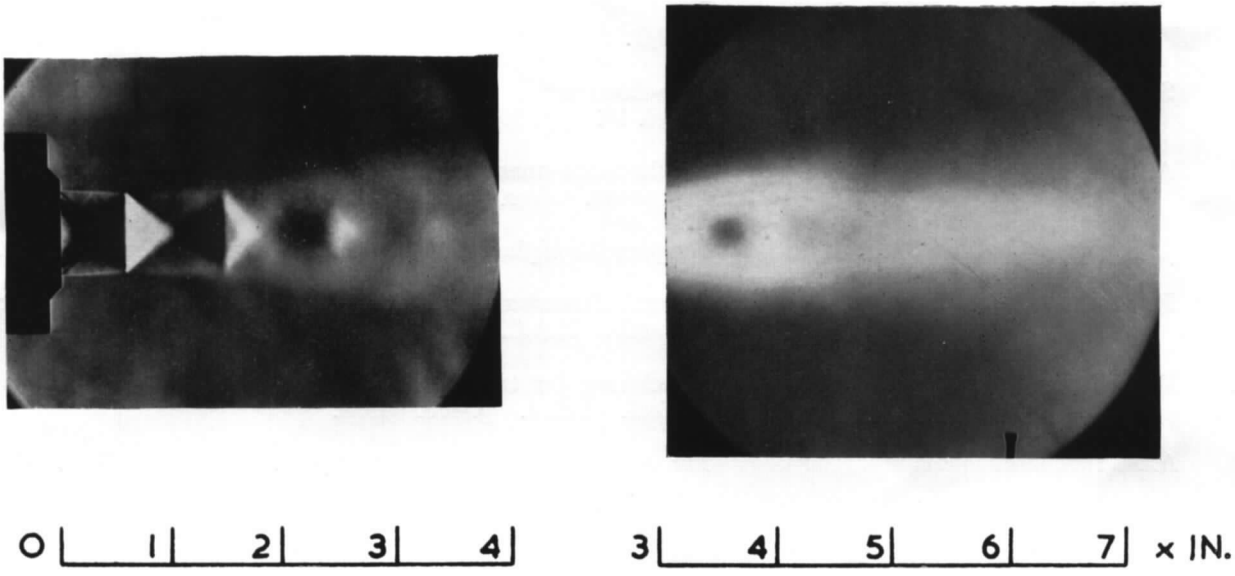

FIG. 2. Jet 1. Schlieren. Continuous.

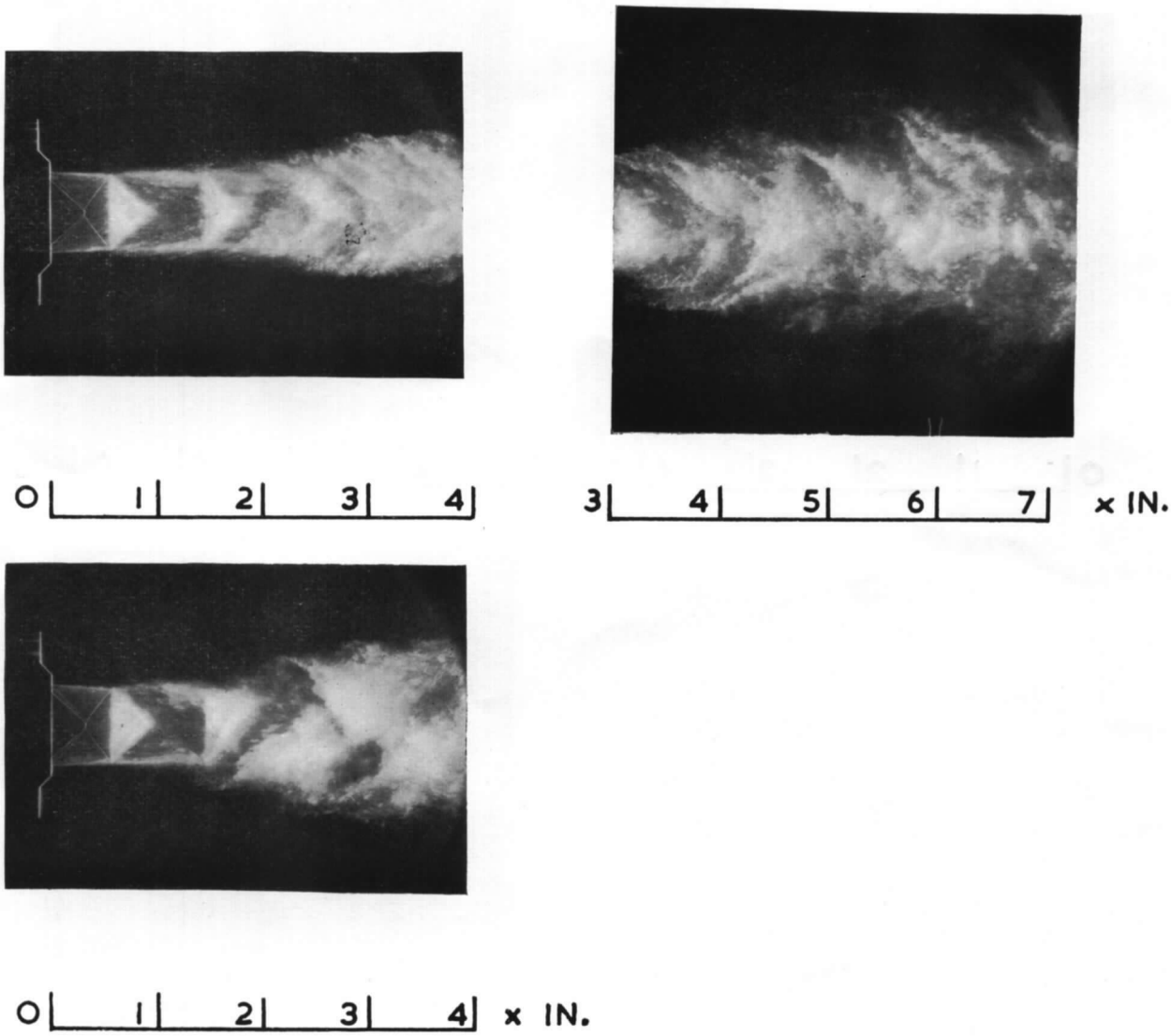

FIG. 3. Jet 1. Schlieren. Flash.

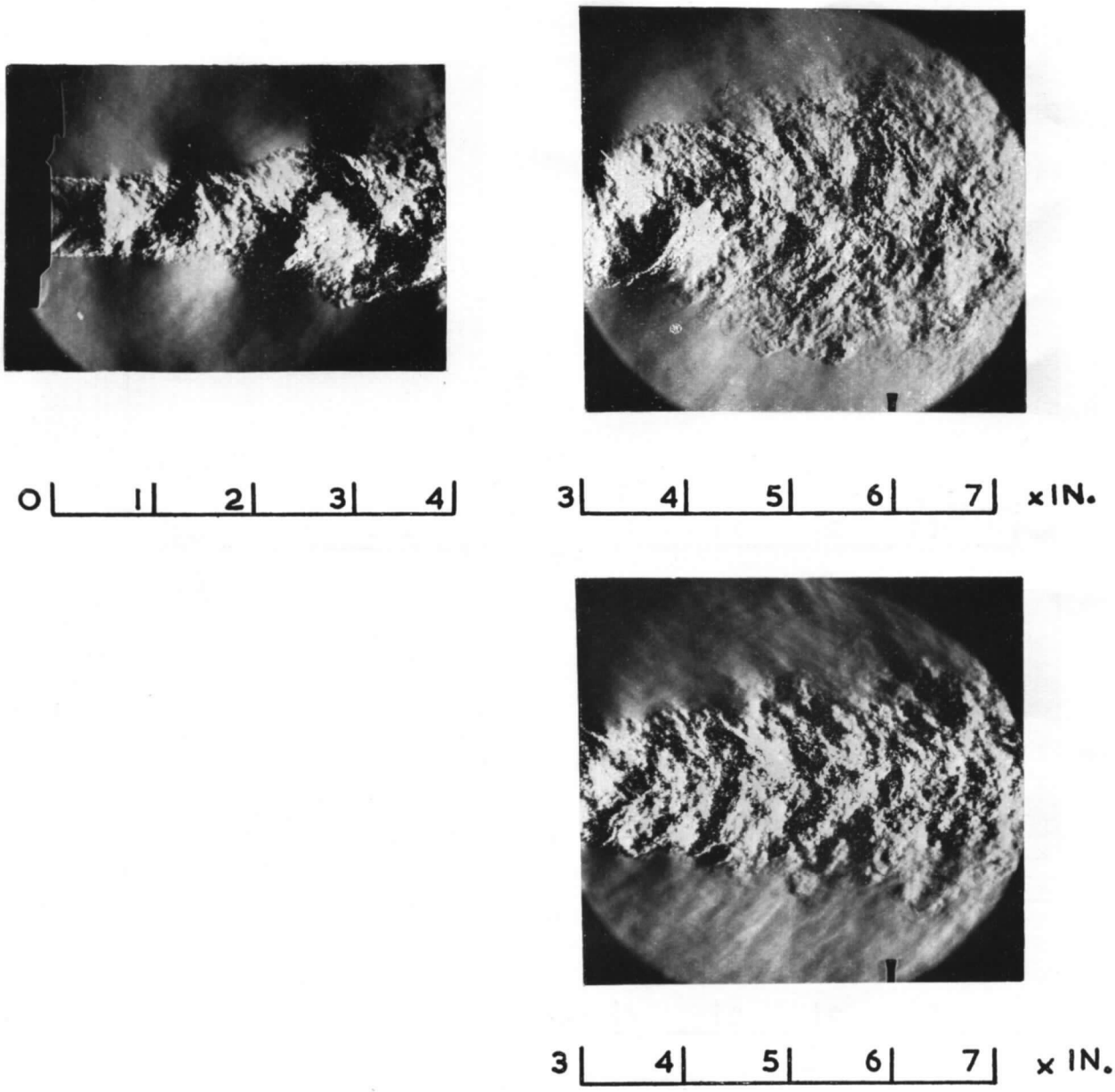

FIG. 4. Jet 1. Schlieren. Spark.

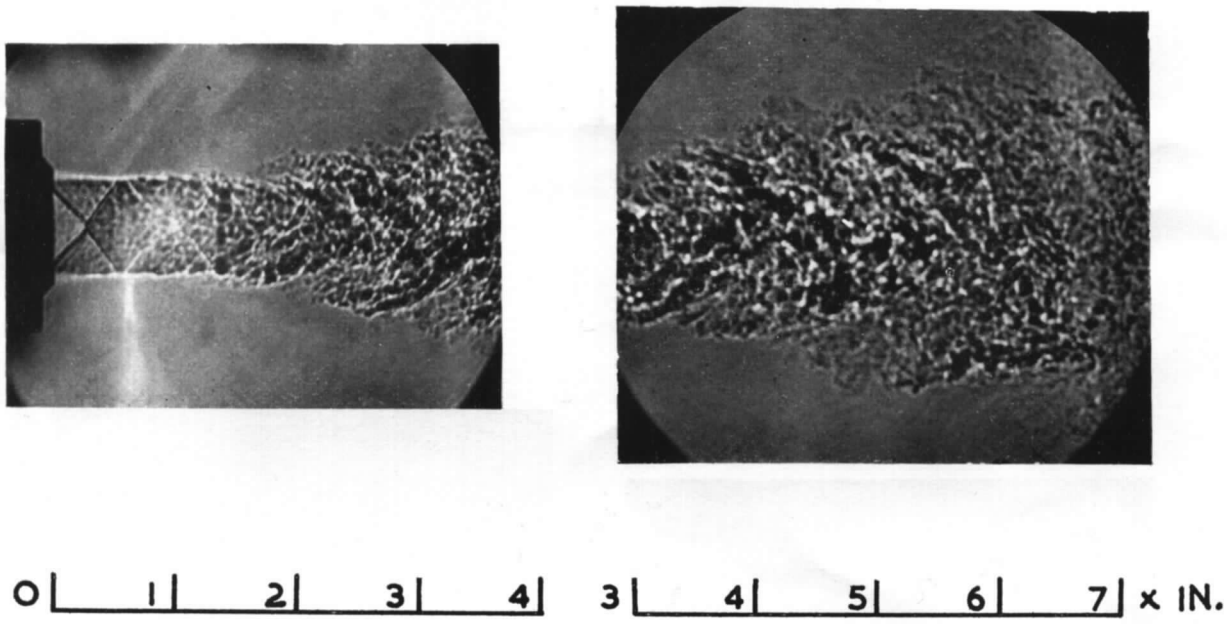

FIG. 5. Jet 1. Shadow. Spark.

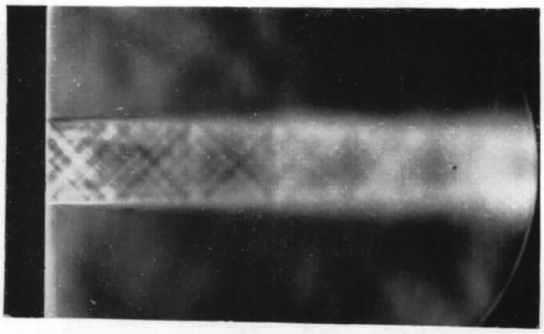

FIG. 6. Jet 6. Schlieren. Continuous.

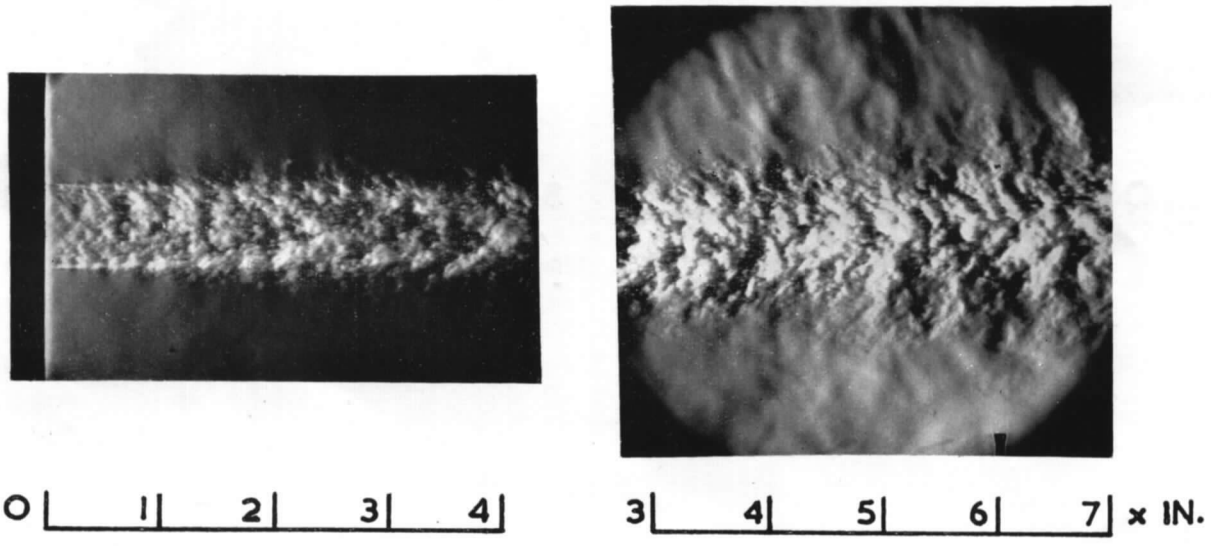

FIG. 7. Jet 6. Schlieren. Flash.

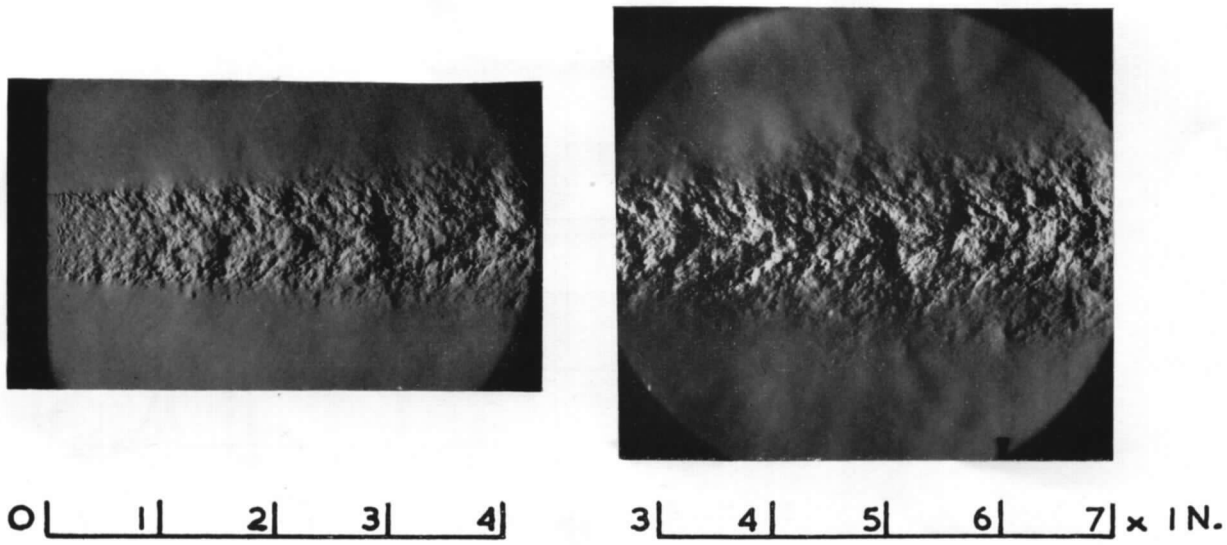

FIG. 8. Jet 6. Schlieren. Spark.

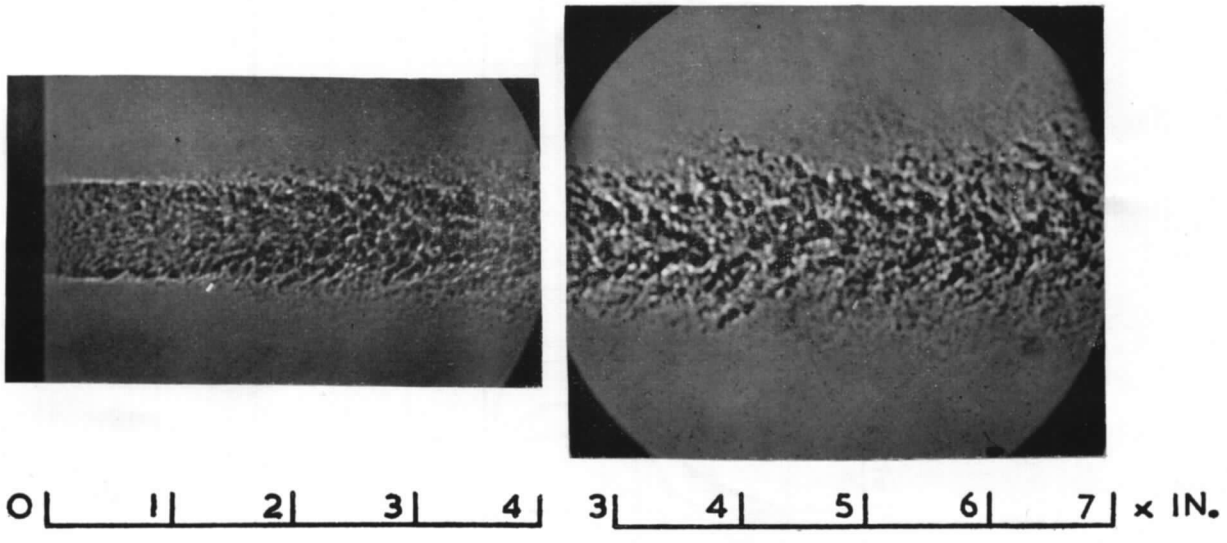

FIG. 9. Jet 6. Shadow. Spark.

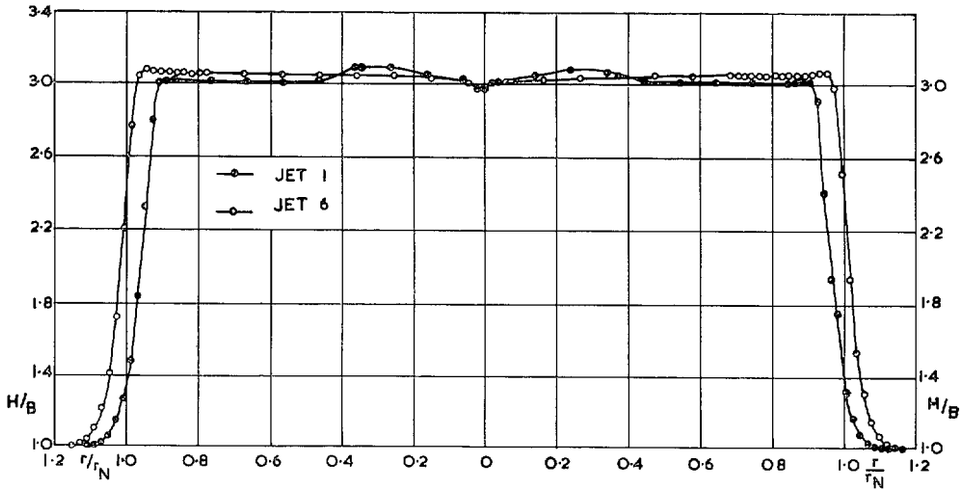

FIG. 10. Pressure traverses at $x = 0{\cdot}4$ in.

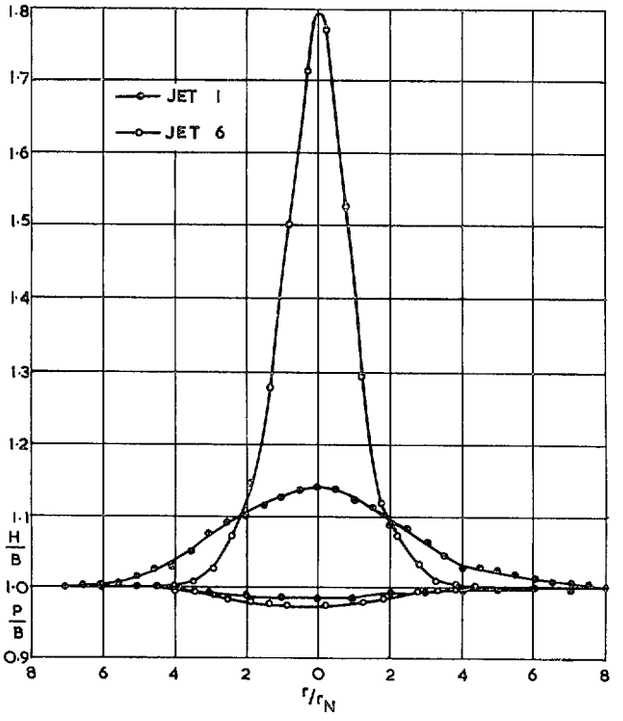

FIG. 11. Pressure traverses at $x = 10{\cdot}0$ in.

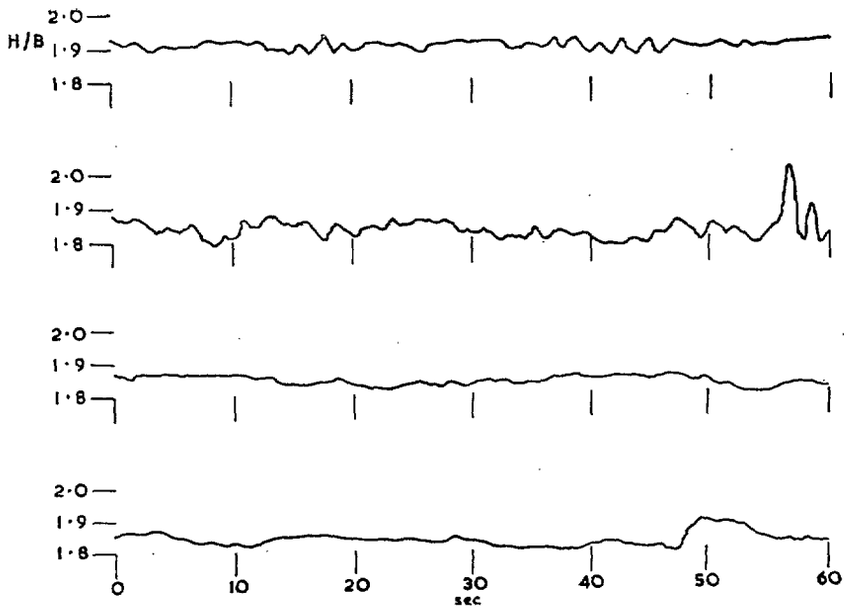

FIG. 12. Pressure records.

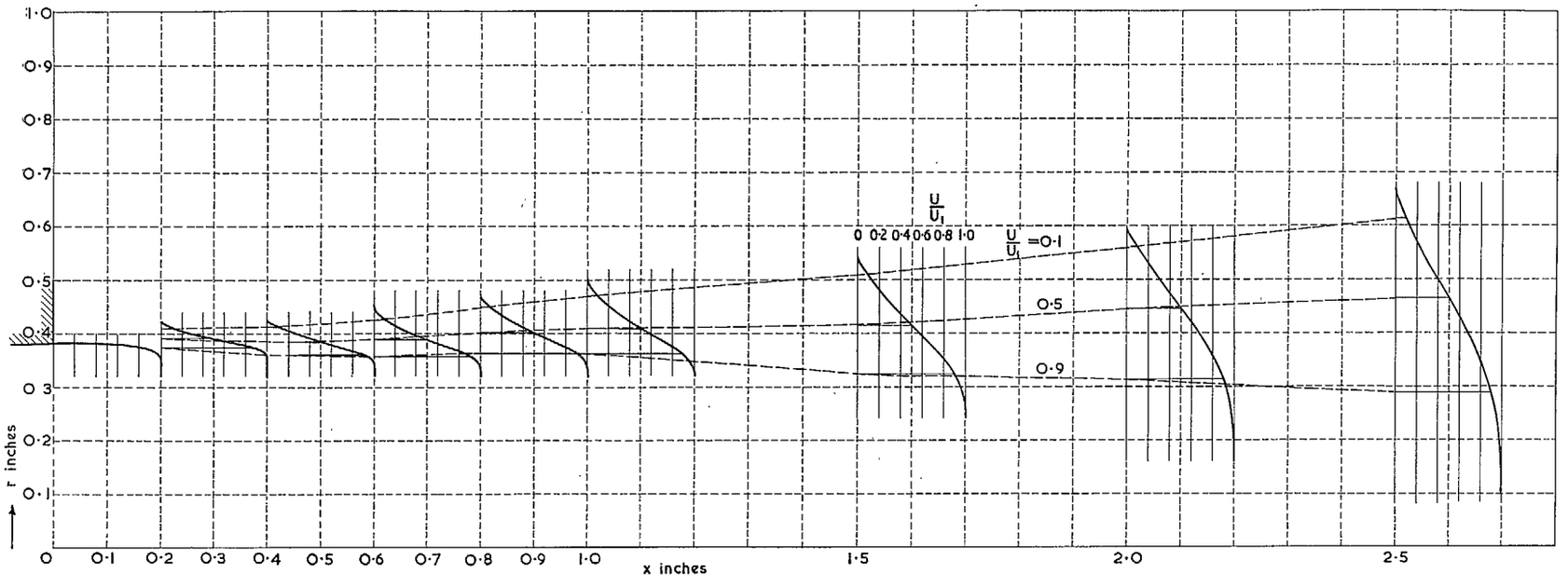

FIG. 13. Jet 1. Velocity profiles.

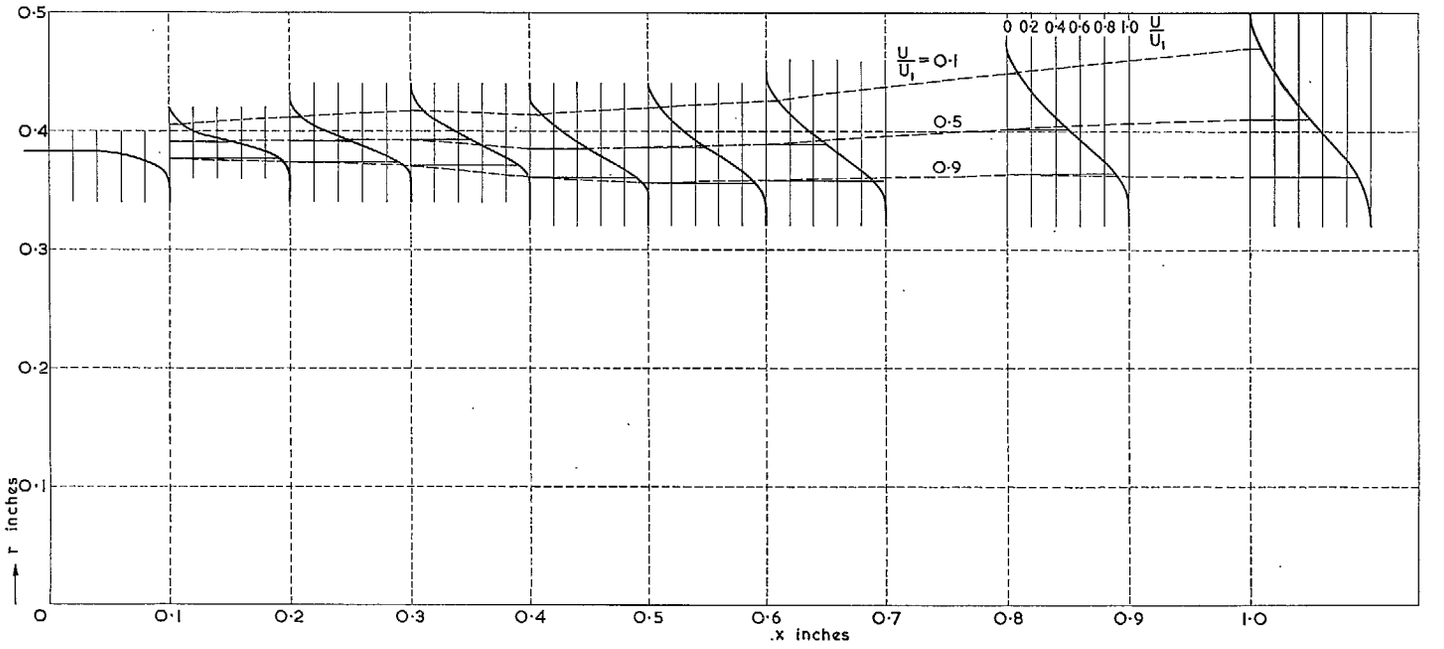

FIG. 14. Jet 1. Velocity profiles.

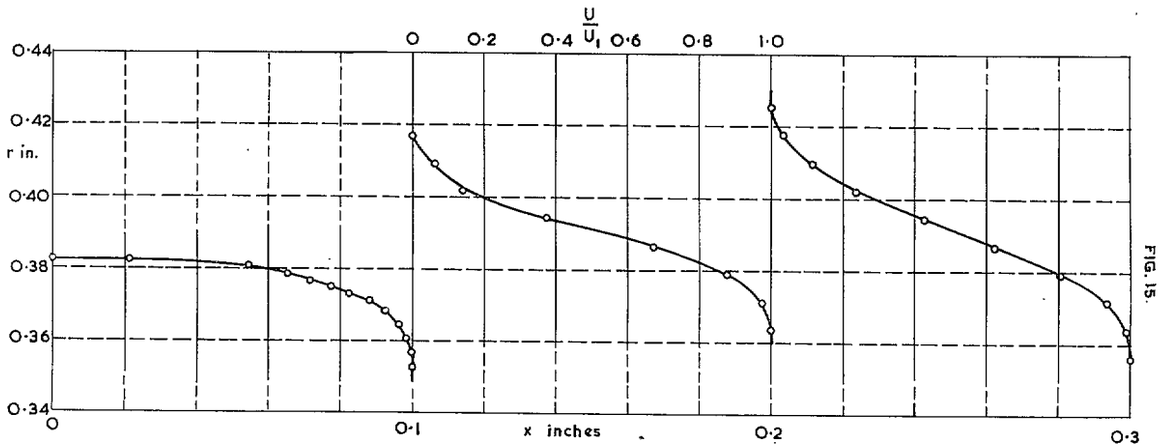

FIG. 15. Jet 1. Velocity profiles.

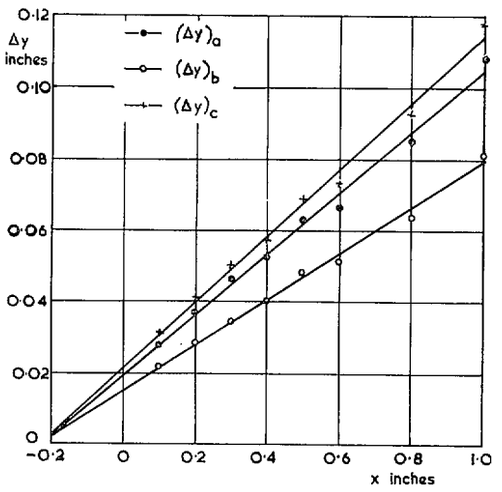

FIG. 16. Mixing-region width, Group I.

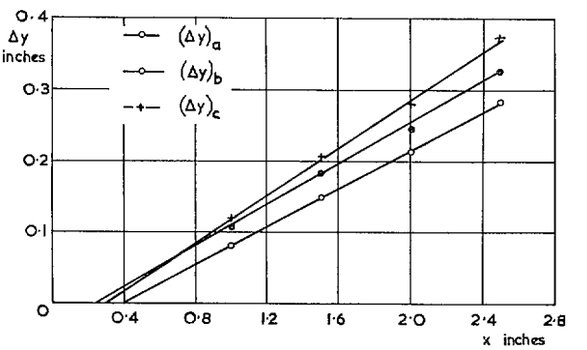

FIG. 17. Mixing-region width, Group II.

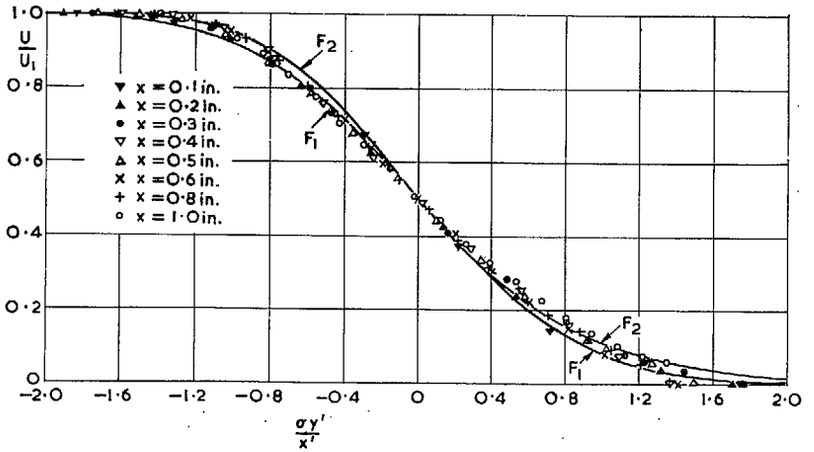

FIG. 18. Similarity of velocity profiles, Group I. $\sigma = 21{\cdot}9$.

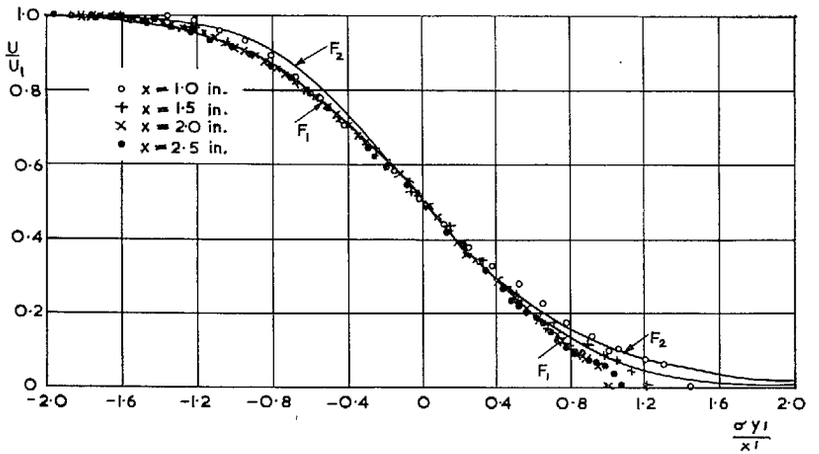

FIG. 19. Similarity of velocity profiles, Group II. $\sigma = 11{\cdot}9$.

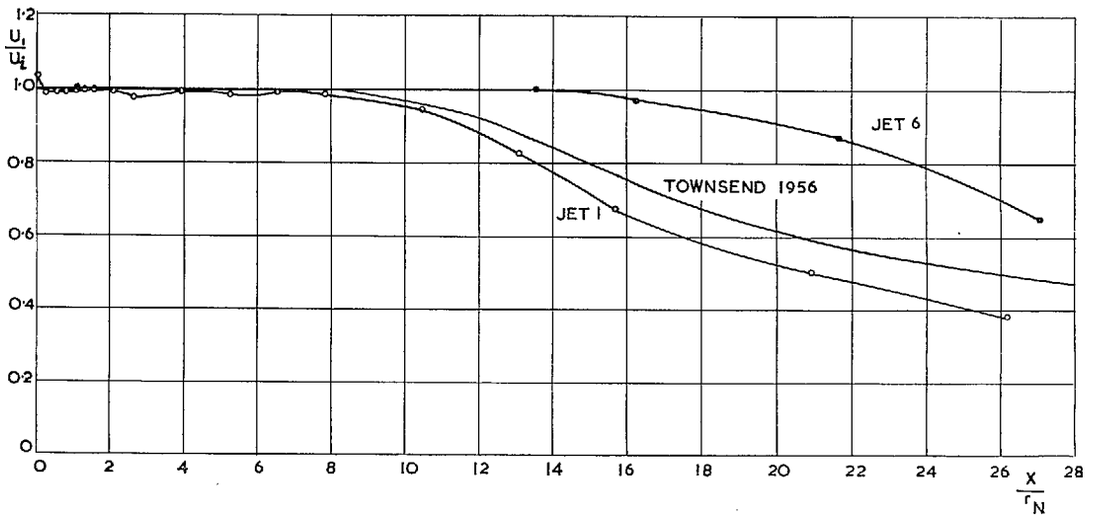

FIG. 20. Velocity on axis.

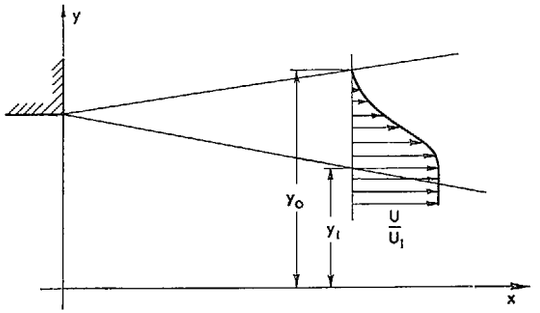

FIG. 21. Two-dimensional half-jet.

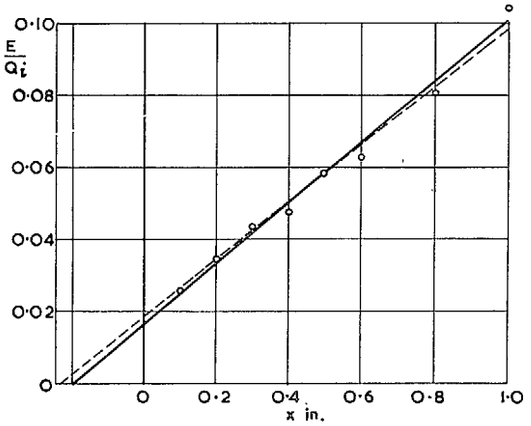

FIG. 23. Entrainment.

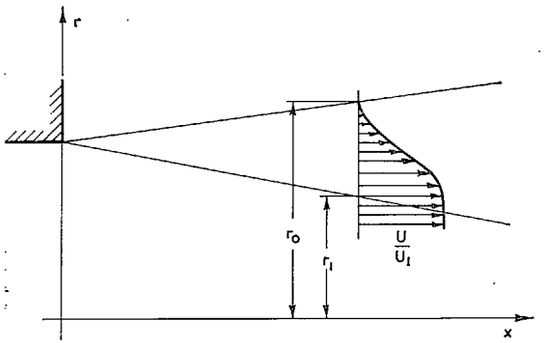

FIG. 22. Axially-symmetrical jet.

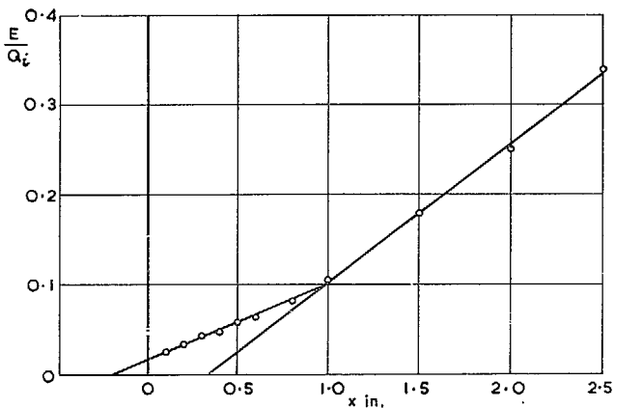

FIG. 24. Entrainment.

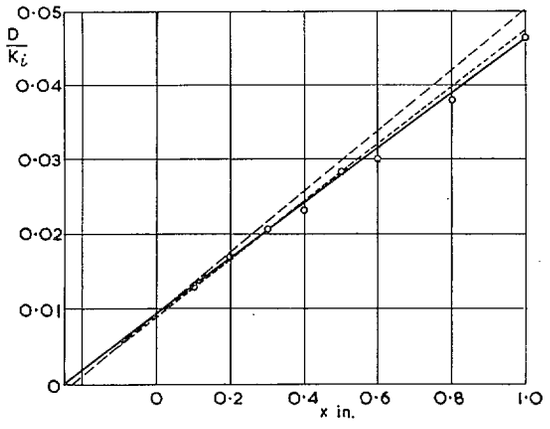

FIG. 25. Loss of kinetic energy.

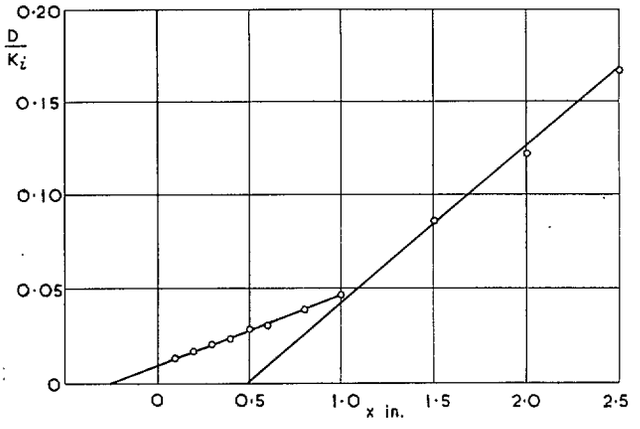

FIG. 26. Loss of kinetic energy.

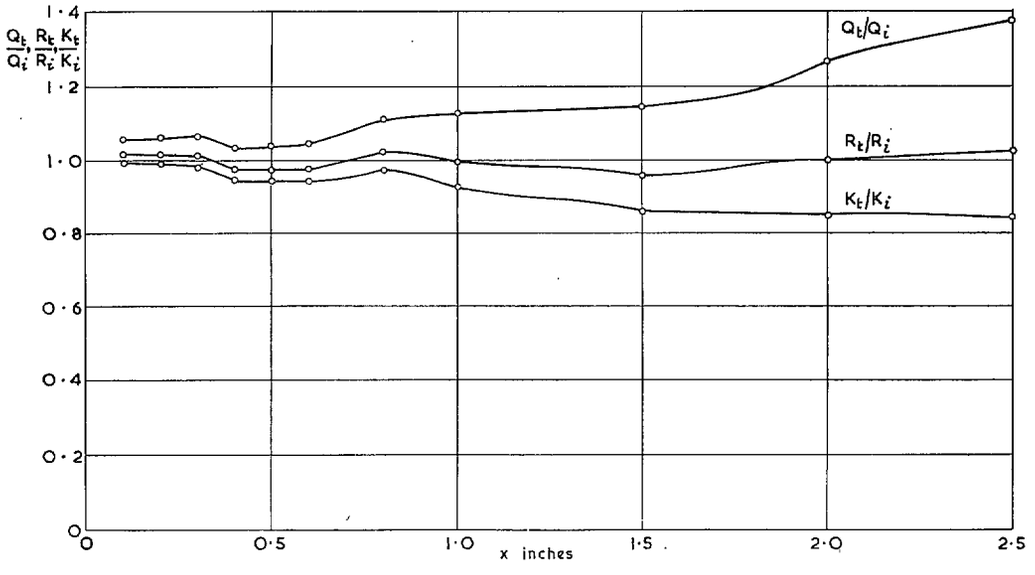

FIG. 27. Total flux.

(85556) Wt. 59/1857 K.5 12/62 Hw.

Publications of the Aeronautical Research Council

ANNUAL TECHNICAL REPORTS OF THE AERONAUTICAL RESEARCH COUNCIL (BOUND VOLUMES)

1942 Vol. I. Aero and Hydrodynamics, Aerofoils, Airscrews, Engines. 75*s.* (post 2*s.* 9*d.*)
Vol. II. Noise, Parachutes, Stability and Control, Structures, Vibration, Wind Tunnels. 47*s.* 6*d.* (post 2*s.* 3*d.*)

1943 Vol. I. Aerodynamics, Aerofoils, Airscrews. 80*s.* (post 2*s.* 6*d.*)
Vol. II. Engines, Flutter, Materials, Parachutes, Performance, Stability and Control, Structures. 90*s.* (post 2*s.* 9*d.*)

1944 Vol. I. Aero and Hydrodynamics, Aerofoils, Aircraft, Airscrews, Controls. 84*s.* (post 3*s.*)
Vol. II. Flutter and Vibration, Materials, Miscellaneous, Navigation, Parachutes, Performance, Plates and Panels, Stability, Structures, Test Equipment, Wind Tunnels. 84*s.* (post 3*s.*)

1945 Vol. I. Aero and Hydrodynamics, Aerofoils. 130*s.* (post 3*s.* 6*d.*)
Vol. II. Aircraft, Airscrews, Controls. 130*s.* (post 3*s.* 6*d.*)
Vol. III. Flutter and Vibration, Instruments, Miscellaneous, Parachutes, Plates and Panels, Propulsion. 130*s.* (post 3*s.* 3*d.*)
Vol. IV. Stability, Structures, Wind Tunnels, Wind Tunnel Technique. 130*s.* (post 3*s.* 3*d.*)

1946 Vol. I. Accidents, Aerodynamics, Aerofoils and Hydrofoils. 168*s.* (post 3*s.* 9*d.*)
Vol. II. Airscrews, Cabin Cooling, Chemical Hazards, Controls, Flames, Flutter, Helicopters, Instruments and Instrumentation, Interference, Jets, Miscellaneous, Parachutes. 168*s.* (post 3*s.* 3*d.*)
Vol. III. Performance, Propulsion, Seaplanes, Stability, Structures, Wind Tunnels. 168*s.* (post 3*s.* 6*d.*)

1947 Vol. I. Aerodynamics, Aerofoils, Aircraft. 168*s.* (post 3*s.* 9*d.*)
Vol. II. Airscrews and Rotors, Controls, Flutter, Materials, Miscellaneous, Parachutes, Propulsion, Seaplanes, Stability, Structures, Take-off and Landing. 168*s.* (post 3*s.* 9*d.*)

1948 Vol. I. Aerodynamics, Aerofoils, Aircraft, Airscrews, Controls, Flutter and Vibration, Helicopters, Instruments, Propulsion, Seaplane, Stability, Structures, Wind Tunnels. 130*s.* (post 3*s.* 3*d.*)
Vol. II. Aerodynamics, Aerofoils, Aircraft, Airscrews, Controls, Flutter and Vibration, Helicopters, Instruments, Propulsion, Seaplane, Stability, Structures, Wind Tunnels. 110*s.* (post 3*s.* 3*d.*)

Annual Reports of the Aeronautical Research Council—

1939–48 3*s.* (post 6*d.*) 1949–54 5*s.* (post 5*d.*)

Index to all Reports and Memoranda published in the Annual Technical Reports, and separately—

April, 1950 – – – – R. & M. 2600 (out of print)

Published Reports and Memoranda of the Aeronautical Research Council—

Between Nos. 2351–2449	R. & M. No. 2450 2*s.* (post 3*d.*)
Between Nos. 2451–2549	R. & M. No. 2550 2*s.* 6*d.* (post 3*d.*)
Between Nos. 2551–2649	R. & M. No. 2650 2*s.* 6*d.* (post 3*d.*)
Between Nos. 2651–2749	R. & M. No. 2750 2*s.* 6*d.* (post 3*d.*)
Between Nos. 2751–2849	R. & M. No. 2850 2*s.* 6*d.* (post 3*d.*)
Between Nos. 2851–2949	R. & M. No. 2950 3*s.* (post 3*d.*)
Between Nos. 2951–3049	R. & M. No. 3050 3*s.* 6*d.* (post 3*d.*)
Between Nos. 3051–3149	R. & M. No. 3150 3*s.* 6*d.* (post 3*d.*)

HER MAJESTY'S STATIONERY OFFICE

York House, Kingsway, London W.C.2; 423 Oxford Street, London W.1; 13a Castle Street, Edinburgh 2; 39 King Street, Manchester 2; 35 Smallbrook, Ringway, Birmingham 5; 109 St. Mary Street, Cardiff; 50 Fairfax Street, Bristol 1; 80 Chichester Street, Belfast 1, *or through any bookseller.*

S.O. Code No. 23-3291